



## Processing and characterizations of BNT-KNN ceramics for actuator applications

Mallam Chandrasekhar, Pawan Kumar\*

Department of Physics and Astronomy, National Institute of Technology, Rourkela, 769008 Odisha, India

Received 22 February 2016; Received in revised form 24 May 2016; Accepted 13 June 2016

### Abstract

*BNT-KNN powder (with composition  $0.93\text{Bi}_{0.5}\text{Na}_{0.5}\text{TiO}_3-0.07\text{K}_{0.5}\text{Na}_{0.5}\text{NbO}_3$ ) was synthesized as a single perovskite phase by conventional solid state reaction route and dense ceramics were obtained by sintering of powder compacts at  $1100^\circ\text{C}$  for 4 h. Dielectric study confirmed relaxor behaviour, whereas the microstructure study showed sharp cornered cubic like grains with an average grain size  $\sim 1.15\ \mu\text{m}$ . The saturated polarization vs. electric field (P-E) hysteresis loops confirmed the ferroelectric (FE) nature while the butterfly shaped strain vs. electric field (S-E) loops suggested the piezoelectric nature of the BNT-KNN ceramic samples. Maximum electric field induced strain of  $\sim 0.62\%$  suggested the usefulness of this system for actuator applications.*

**Keywords:** actuator, electron microscopy, relaxor ferroelectrics, microstructure, thermal analysis

### I. Introduction

Electric field induced strain in a functional material can be related to piezoelectric or electrostrictive phenomena [1]. A piezoelectric material with high electric field induced strain is useful in various actuator based applications like: fuel injectors, ink cartridges, ultrasonic motors, etc. In piezoelectric materials, the electric field induced strain is accounted in terms of: (i) extrinsic contribution due to non- $180^\circ$  domain switching and (ii) intrinsic contribution due to the change in the dimension of the unit cell.  $\text{Bi}_{0.5}\text{Na}_{0.5}\text{TiO}_3$  (BNT) system shows good ferroelectric (FE) and piezoelectric properties at room temperature (RT), but there are some critical issues associated with this system such as: high coercive field ( $E_c$ ) and high Curie's temperature ( $T_c$ ), which goes against the use of this system in various device applications [2]. To overcome these disadvantages, binary solid solutions of BNT with  $\text{BaTiO}_3$  (BT),  $\text{K}_{0.5}\text{Na}_{0.5}\text{NbO}_3$  (KNN) etc. systems have been proposed [3]. A ferroelectric system exhibits optimum performance near the morphotropic phase boundary (MPB) compositions [4]. In BNT-KNN system, near RT there exists MPB and FE to AFE phase transition temperature, known as depolarization temperature ( $T_d$ ) [3].

Near  $T_d$  BNT-KNN system undergoes transition from FE to anti-ferroelectric (AFE) phase, which results in dimensional change and high electric field induced strain [2].

In the present study, 0.93BNT-0.07KNN powder was synthesized as a single perovskite phase and sintered into dense ceramics. Its structural, dielectric and electric field induced polarization and strain properties were studied.

### II. Material and methods

BNT-KNN ( $0.93\text{Bi}_{0.5}\text{Na}_{0.5}\text{TiO}_3-0.07\text{K}_{0.5}\text{Na}_{0.5}\text{NbO}_3$ ) powder was prepared using conventional solid-state reaction route. Stoichiometric proportion of  $\text{Bi}_2\text{O}_3$ ,  $\text{TiO}_2$ ,  $\text{Nb}_2\text{O}_5$ ,  $\text{Na}_2\text{CO}_3$ ,  $\text{BaCO}_3$  and  $\text{K}_2\text{CO}_3$  precursors (all with 99.9% purity) was taken into a jar and ball milled for 20 h in acetone using zirconia balls as the grinding media. Calcination temperature of the BNT-KNN sample was estimated by differential scanning calorimetry - thermo gravimetric analysis (DSC-TGA) of the dried ball milled powder in the temperature range of RT to  $1000^\circ\text{C}$  with a heating rate of  $5^\circ\text{C}$  per minute using thermal analyser (Netzsch, Germany STA449C/4/MFC/G). Subsequently, calcination was carried out at  $850^\circ\text{C}$  for 4 h in air and the single perovskite phase formation was confirmed by powder X-ray diffraction technique (Rigaku Ultima IV). Polyvinyl alcohol binder solution (3 wt.%) was added to the cal-

\*Corresponding author: tel: +91 661-2462726, fax: +91 661-2462726, e-mail: pvn77@rediffmail.com, pawankumar@nitrkl.ac.in

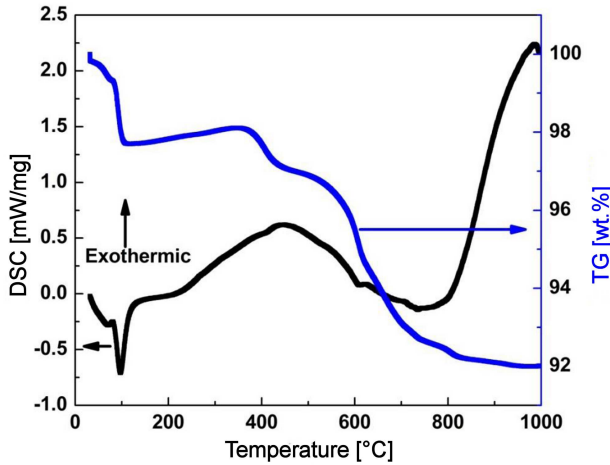


Figure 1. DSC-TGA plot of the uncalcined BNT-KNN powder

cined powder and compressed into pellets of ~10 mm in diameter and ~1.5 mm in thickness, using a hydraulic press with 10 MPa pressure. The green pellets were sintered at 1100 °C for 4 h. For electrical measurements, silver paste was deposited on both sides of the sintered pellets followed by firing at 400 °C for 30 minutes. Sintered pellet micrograph was taken using field emission scanning electron microscope (NOVA nano SEM). Dielectric constant ( $\epsilon_r$ ) and dielectric loss ( $\tan \delta$ ) variation with frequency and temperature were carried out using HIOKI 3532-50 LCR tester. RT polarization vs. electric field and strain vs. electric field and temperature dependent polarization vs. electric field behaviours were studied using Radiant precision premier II and with attached MTI-2100 Fotonic sensor, respectively.

### III. Results and discussion

DSC and TGA plots of the uncalcined BNT-KNN powder, shown in Fig. 1, represent the variation of heat flow in/out and the weight loss percentage with the

change in temperature, respectively. In DSC plot, the heat flowing out of the samples points towards exothermic peak, whereas the heat flowing into the samples points towards endothermic peak [5]. TGA plot shows ~8% overall weight loss from RT to 1000 °C. Distinctly, TGA plot has two major weight loss regions, the first one of ~3% in temperature range between RT and 130 °C, while the second one of ~5% in temperature range between 220 and 730 °C. The first weight loss region can be related to vaporization of water [6,7], whereas the second weight loss region can be accounted in terms of decomposition of the starting precursors. Corresponding to these two weight loss regions, endothermic and exothermic peaks were observed in the DSC plot. A small weight loss in the 800 to 1000 °C temperature range corresponds to an exothermic peak in DSC plot, which can be related to the crystallization temperature of the BNT-KNN sample [8,9].

Figure 2 shows the XRD pattern and the deconvolution of the 200 peak of the sintered BNT-KNN ceramic samples. The XRD peaks confirm development of single perovskite phase, whereas sharp peaks indicate high crystallinity of the sintered BNT-KNN ceramic samples [10]. Deconvolution of the XRD peak 200, shown in Fig. 2b, suggests the presence of ~53% of rhombohedral and ~47% of tetragonal structures in the BNT-KNN ceramic samples. Rhombohedral phase (*R.P*) and tetragonal phase (*T.P*) fractions [11] in the sintered sample are calculated by using the following relations:

$$T.P = \frac{I_{200_r} + I_{002_T}}{I_{200_r} + I_{002_T} + I_{200_N}} \quad (1)$$

$$R.P = 1 - T.P = \frac{I_{200_N}}{I_{200_r} + I_{002_T} + I_{200_N}} \quad (2)$$

where, *I* is the integral intensity of the corresponding XRD peak. Occurrence of double structure suggests the MPB nature of the BNT-KNN ceramic samples [3,9]. Lattice parameters of rhombohedral crystal structure are

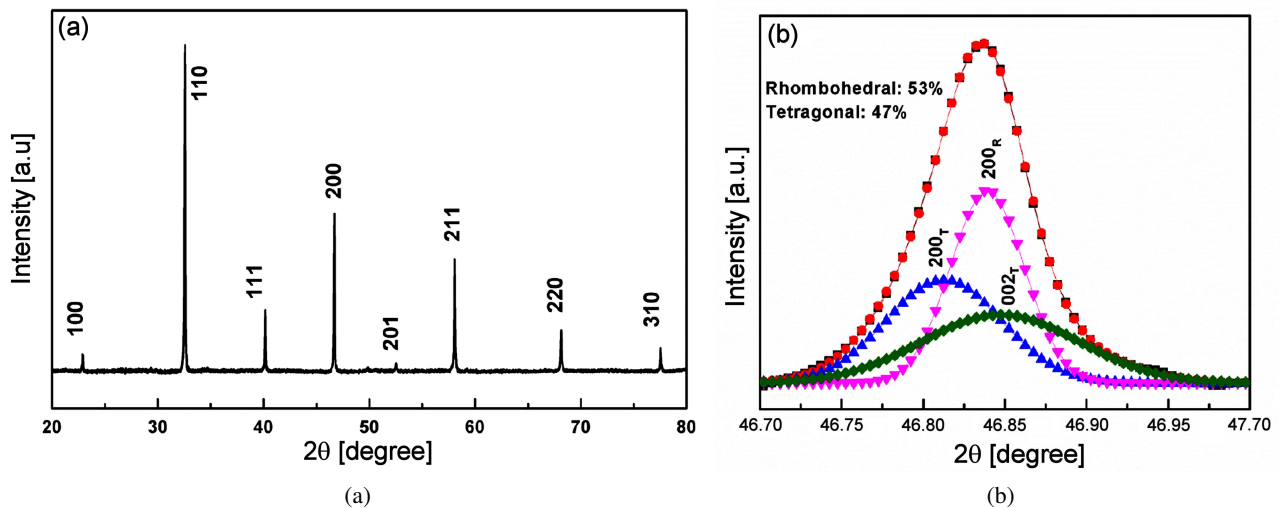


Figure 2. XRD pattern (a) and deconvolution of XRD peak 200 (b) of the BNT-KNN ceramic samples

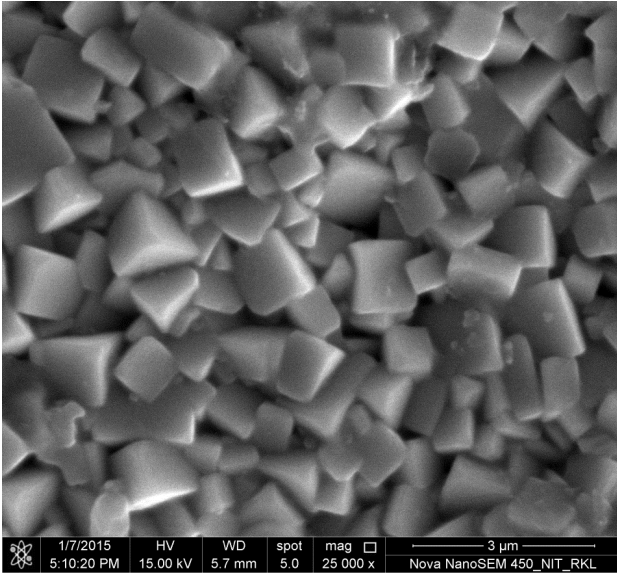
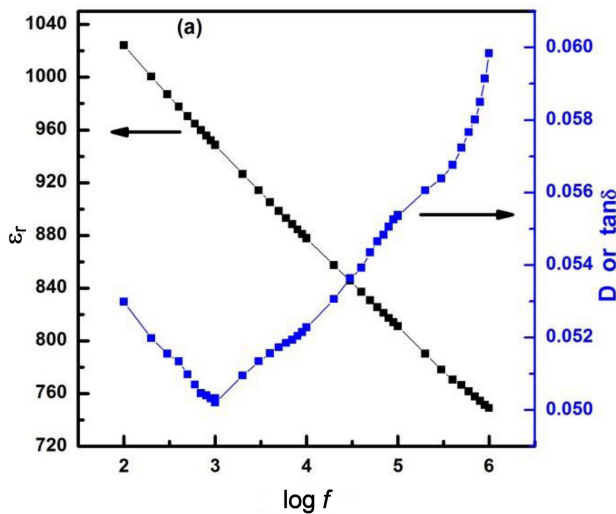


Figure 3. FESEM micrograph of the BNT-KNN ceramic samples

$a = b = c = 5.4974 \text{ \AA}$ ,  $\alpha = \beta = \gamma = 90.08^\circ$  with unit cell volume  $\sim 166.14 \text{ \AA}^3$ , whereas, for tetragonal crystal structure  $a = b = 5.4998 \text{ \AA}$  and  $c = 13.7274 \text{ \AA}$ ,  $\alpha = \beta = \gamma = 90^\circ$  with unit cell volume  $\sim 415.23 \text{ \AA}^3$ .

Figure 3 shows the FESEM micrograph of the sintered BNT-KNN ceramic samples. The microstructure reveals the dense, uniformly distributed and tightly bounded sharp cornered cubic like grains. The average grain size, calculated using linear intercept method [12], was found to be  $\sim 1.15 \mu\text{m}$ .

Figure 4a shows the variation of  $\epsilon_r$  with frequency. Decrease of  $\epsilon_r$  with the increase of frequency can be related to the decrease of net polarization [9]. Figure 4a also shows the increase of  $\tan \delta$  with the increase of frequency. At lower frequencies, all the polarizations follow the varying AC field; whereas at higher frequencies the dielectric relaxation processes sets in the BNT-KNN ceramic samples, which lead to an increase in dielec-



tric loss with the increase of frequency [9,13]. Figure 4b shows two dielectric anomalies in the dielectric constant vs. temperature ( $\epsilon_r$ - $T$ ) plot of the BNT-KNN ceramic samples. The first dielectric anomaly at  $\sim 125^\circ\text{C}$  is attributed to the depolarization temperature ( $T_d$ ) [14], whereas the second dielectric anomaly at  $\sim 300^\circ\text{C}$ , corresponds to the Curie temperature  $T_c/T_m$ , which is related to the maximum dielectric constant [9,13,15]. This suggests that AFE phase exists in the  $125$ – $300^\circ\text{C}$  temperature range and pinched  $P$ - $E$  hysteresis loops should appear in the  $T_d$  to  $T_c$  temperature range.  $T_m$  is found to be frequency dependent, i.e. there is a shift towards higher temperature side with the increase of frequency, which is a typical characteristic of relaxor ferroelectric materials. This relaxor nature may be attributed to the dynamics of the A-site ions in the BNT-KNN system [9,16].

Figure 5 shows the RT polarization and induced strain vs. electric field hysteresis loops (at 10 Hz frequency) of the BNT-KNN ceramic samples. Well saturated  $P$ - $E$  hysteresis loop with a maximum polarization ( $P_m$ ) of  $\sim 31 \mu\text{C}/\text{cm}^2$ , remnant polarization ( $P_r$ ) of  $\sim 20 \mu\text{C}/\text{cm}^2$  and coercive field ( $E_c$ ) of  $\sim 26 \text{ kV}/\text{cm}$  are observed. Well saturated  $P$ - $E$  loop indicates the FE nature of BNT-KNN system at RT [8], also confirmed by the butterfly shaped  $S$ - $E$  loop [4,17]. The butterfly shaped  $S$ - $E$  loop is formed due to converse piezoelectric effect, switching and movement of the domain walls [17]. From the RT  $S$ - $E$  loop (Fig. 5) it can be seen that maximum induced strain of  $\sim 0.62\%$  and remnant strain of  $\sim 0.18\%$  are obtained. Asymmetry in the  $S$ - $E$  loop may be attributed to the back switching of the domains during bipolar cycling of the applied external electric field. This back switching of domains during bipolar cycling accounts polar order at zero electric field, which results in the asymmetry of  $S$ - $E$  loops [18].

The  $P$ - $E$  loops at different temperatures are shown in Fig. 6. Ferroelectricity of the BNT-KNN ceramic samples decreases with the increase of temperature. This can be related to the decrease in interface energy of FE

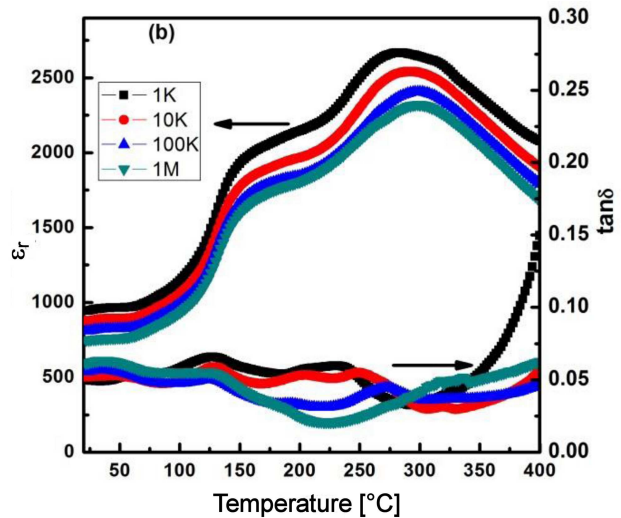


Figure 4. Variation of  $\epsilon_r$  and  $\tan \delta$  with (a) frequency ( $f$ ) and (b) temperature of the BNT-KNN ceramic samples

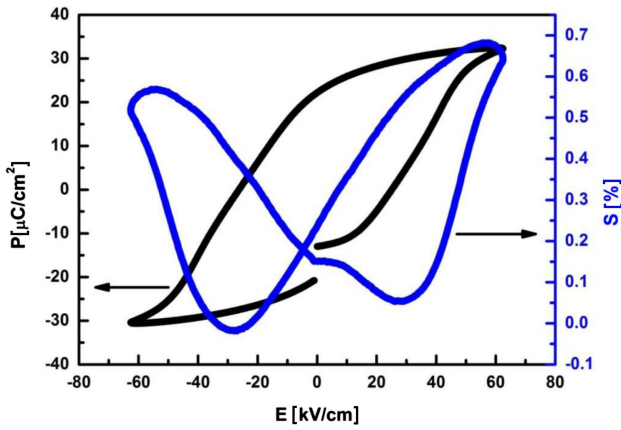


Figure 5. Bipolar  $P$ - $E$  and  $S$ - $E$  loops of the BNT-KNN ceramic samples

domains, which results in the easier domain wall movement and slim  $P$ - $E$  loops [13,19]. When the temperature is  $\geq 140^\circ\text{C}$ , which corresponds to FE-AFE transition temperature ( $T_d$ ), deformed and pinched  $P$ - $E$  hysteresis loops start appearing.

#### IV. Conclusions

Single perovskite phase BNT-KNN lead free ceramic samples (with composition  $0.93\text{Bi}_{0.5}\text{Na}_{0.5}\text{TiO}_3$ - $0.07\text{K}_{0.5}\text{Na}_{0.5}\text{NbO}_3$ ) were prepared by conventional solid state reaction route. Deconvolution of 200 XRD peak revealed its MPB nature with 53% of rhombohedral and 47% of tetragonal structures. FESEM micrograph showed dense and uniform distribution of grains. Dielectric study confirmed the relaxor nature of BNT-KNN ceramic samples. Transformation of FE to AFE

phase was confirmed separately by temperature dependence dielectric and temperature dependent  $P$ - $E$  loop studies, respectively. High strain of  $\sim 0.62\%$  suggested the usefulness of BNT-KNN system for actuator applications.

#### References

1. K. Uchino, *Piezoelectric Actuators and Ultrasonic Motors*, Kluwer Academic Publishers, Boston, USA, 1997.
2. S.-T. Zhang, A.B. Kounga, E. Aulbach, W. Jo, T. Granzow, H. Ehrenberg, J. Rödel, "Lead-free piezo ceramics with giant strain in the system  $\text{Bi}_{0.5}\text{Na}_{0.5}\text{TiO}_3$ - $\text{BaTiO}_3$ - $\text{K}_{0.5}\text{Na}_{0.5}\text{NbO}_3$ . II. Temperature dependent properties", *J. Appl. Phys.*, **103** (2008) 034108-7.
3. A.B. Kounga, S.-T. Zhang, W. Jo, T. Granzow, J. Rödel, "Morphotropic phase boundary in  $(1-x)\text{Bi}_{0.5}\text{Na}_{0.5}\text{TiO}_3$ - $x\text{K}_{0.5}\text{Na}_{0.5}\text{NbO}_3$  lead-free piezoceramics", *Appl. Phys. Lett.*, **92** (2008) 222902-3.
4. S. Zhang, R. Xia, T.R. Shrout, "Modified  $(\text{K}_{0.5}\text{Na}_{0.5})\text{NbO}_3$  based lead-free piezoelectrics with broad temperature usage range", *Appl. Phys. Lett.*, **91** (2007) 132913-3.
5. P. Gabbott, *The Principles and Applications of Thermal Analysis*, Wiley-Blackwell, London, UK, 2007.
6. A. Chaouchi, S. Kennour, S. d'Astorg, M. Rguiti, C. Courtois, S. Marinell, M. Aliouat, "Characterization of sol-gel synthesised lead-free  $(1-x)\text{Na}_{0.5}\text{Bi}_{0.5}\text{TiO}_3$ - $x\text{BaTiO}_3$ -based ceramics", *J. Alloys Compd.*, **509** (2011) 9138–9143.
7. Sonia, M. Chandrasekhar, P. Kumar, "Microwave sintered sol-gel derived  $\text{BaTiO}_3$  and

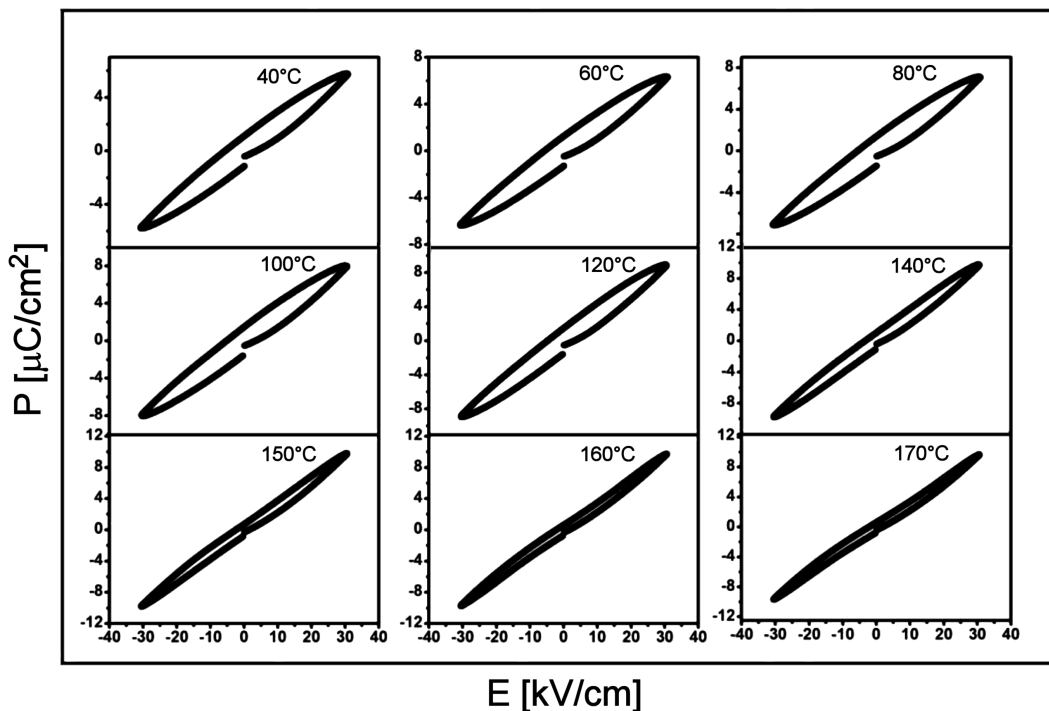


Figure 6.  $P$ - $E$  hysteresis loop at different temperatures of the BNT-KNN ceramic samples

- Ba<sub>0.95</sub>La<sub>0.05</sub>TiO<sub>3</sub> ceramic samples for capacitor applications”, *Ceram. Int.*, **42** (2016) 10587–10592.
8. Z.-M. Wang, K. Zhao, X.-L. Guo, W. Sun, H.-L. Jiang, X.-G. Han, X.-T. Tao, Z.-X. Cheng, H.-Y. Zhao, H. Kimura, G.-L. Yuan, J. Yin, Z.-G. Liu, “Crystallization, phase evolution and ferroelectric properties of sol-gel synthesized Ba(Ti<sub>0.8</sub>Zr<sub>0.2</sub>)O<sub>3</sub>–x(Ba<sub>0.7</sub>Ca<sub>0.3</sub>)TiO<sub>3</sub> thin films”, *J. Mater. Chem. C*, **1** (2013) 522–530.
  9. M. Chandrasekhar, P. Kumar, “Synthesis and characterizations of BNT–BT–KNN ceramics for energy storage applications”, *Phase Transitions, in print*, DOI:10.1080/01411594.2015.1118763
  10. W. Bai, J. Hao, F. Fu, W. Li, B. Shen, J. Zhai, “Structure and strain behavior of <001> textured BNT-based ceramics by template grain growth”, *Mater. Lett.*, **97** (2013) 137–140.
  11. M.-P. Zheng, Y.-D. Hou, H.-Y. Ge, M.-K. Zhu, H. Yan, “Effect of NiO additive on microstructure, mechanical behaviour and electrical properties of 0.2PZN–0.8PZT ceramics”, *J. Eur. Ceram. Soc.*, **33** (2013) 1447–1456.
  12. W.D. Callister, D.G. Rethwisch, *Fundamentals of Materials Science and Engineering: An Introduction*, 8<sup>th</sup> Edition, John Wiley & Sons, USA, 2008.
  13. M. Chandrasekhar, P. Kumar, “Synthesis and characterizations of BNT–BT and BNT–BT–KNN ceramics for actuator and energy storage applications”, *Ceram. Int.*, **41** (2015) 5574–5580.
  14. S.-T. Zhang, A.B. Kounga, E. Aulbach, T. Granzow, W. Jo, H.-J. Kleebe, J. Rödel, “Lead-free piezoceramics with giant strain in the system Bi<sub>0.5</sub>Na<sub>0.5</sub>TiO<sub>3</sub>–BaTiO<sub>3</sub>–K<sub>0.5</sub>Na<sub>0.5</sub>NbO<sub>3</sub>. I. Structure and room temperature properties”, *J. Appl. Phys.*, **103** (2008) 034107-8.
  15. I. Bretos, D. Alonso-San Jose, R. Jimenez, J. Ricote, M. Lourdes Calzada, “Evidence of morphotropic phase boundary displacement in lead-free (Bi<sub>0.5</sub>Na<sub>0.5</sub>)<sub>1-x</sub>Ba<sub>x</sub>TiO<sub>3</sub> polycrystalline thin films”, *Mater. Lett.*, **65** (2011) 2714–2716.
  16. K. Kumar, B.K. Singh, M.K. Gupta, N. Sinha, B. Kumar, “Enhancement in dielectric and ferroelectric properties of lead free Bi<sub>0.5</sub>(Na<sub>0.5</sub>K<sub>0.5</sub>)<sub>0.5</sub>TiO<sub>3</sub> ceramics by Sb-doping”, *Ceram. Int.*, **37** (2011) 2997–3004.
  17. H.-S. Han, C.-W. Ahn, I.W. Kim, A. Hussain, J.-S. Lee, “Destabilization of ferroelectric order in bismuth perovskite ceramics by A-site vacancies”, *Mater. Lett.*, **70** (2012) 98–100.
  18. T.Y. Ansell, D.P. Cann, “High temperature piezoelectric ceramics based on (1-x) [BiScO<sub>3</sub> + Bi(Ni<sub>1/2</sub>Ti<sub>1/2</sub>)O<sub>3</sub>]-xPbTiO<sub>3</sub>”, *Mater. Lett.*, **80** (2012) 87–90.
  19. A.K. Nath, N. Medhi, “Piezoelectric properties of environmental friendly bismuth doped bariumtitanate ceramics”, *Mater. Lett.*, **73** (2012) 75–77.

